Cooperative Effects in a Tenuous Energetic Plasma Contained by a Magnetic Mirror Field

C. C. Damm, J. H. Foote, A. H. Futch Jr., A. L. Gardner, F. J. Gordon, A. L. Hunt, and R. F. Post

Citation: Physics of Fluids (1958-1988) **8**, 1472 (1965); doi: 10.1063/1.1761443
View online: http://dx.doi.org/10.1063/1.1761443
View Table of Contents: http://scitation.aip.org/content/aip/journal/pof1/8/8?ver=pdfcov
Published by the AIP Publishing

Cooperative Effects in a Tenuous Energetic Plasma Contained by a Magnetic Mirror Field

C. C. Damm, J. H. Foote, A. H. Futch, Jr., A. L. Gardner, F. J. Gordon, A. L. Hunt, and R. F. Post
Lawrence Radiation Laboratory, University of California, Livermore, California
(Received 12 April 1965)

The formation and characteristics of a steady-state hydrogen plasma contained in a magnetic mirror field are described. The mean ion energy is 20 keV. The plasma is formed by ionizing and trapping a portion of a beam of energetic hydrogen atoms passing through the confining field. The methods of measurement used to determine the plasma properties are described. Measurements of the radial and azimuthal trapped-ion distributions, the average ion and electron densities, and the plasma potential are compared with the predictions of simple theory, neglecting cooperative plasma effects. The observed deviations from these simple predictions show that the plasma properties are dominated by cooperative phenomena. The plasma density is found to be limited to a low value ($\sim 4 \times 10^7$ ions/cm^3) by a flute or drift instability. This instability is characterized by a low frequency rotation of the plasma at a frequency typically close to the ∇B precession frequency of a 20-keV proton in the nonuniform mirror field. The plasma density at the unstable limit is observed to be related to the value of plasma potential. This relationship can be understood quantitatively by an extension of an earlier theoretical treatment of the drift instability to the case of unequal ion and electron densities. The flute oscillation frequency is also derived from this theory. Oscillations at the ion gyrofrequency are observed, marking the presence of an electrostatic resonance type of instability. Coupling of these modes with the flute oscillations is described, but detailed identification of the electrostatic resonance modes cannot yet be made.

I. INTRODUCTION

THIS paper describes the formation and behavior of a low density plasma of high kinetic temperature produced by ionizing a portion of a beam of energetic hydrogen atoms passing through a steady magnetic-mirror confining field. A preliminary description of this experiment, the Lawrence Radiation Laboratory "Alice" experiment, has been published.[1] Because of the strong connection between the method of formation and the properties of the resulting plasma, the apparatus will be described in more detail here. The experimental arrangement is diagrammed schematically in Fig. 1 and discussed in the next section. We also describe the methods of measurement in enough detail to clearly define the limits of validity of the results.

A model of the plasma to be expected in the absence of cooperative plasma phenomena serves as a standard by which to gauge the effects of cooperative motions actually observed. Such a simplified model will now be described.

The 20-keV hydrogen atoms are injected with a very small spread in both direction and energy. Over the range of magnetic fields investigated, the ratio of plasma diameter to proton orbit diameter varies from 3 to 18, and nonadiabatic losses are expected to be negligible.

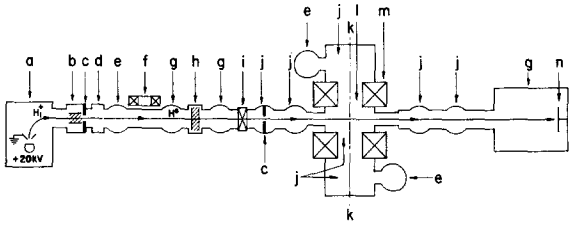

FIG. 1. Schematic drawing of experimental arrangement: (a) ion source, (b) neutralizing cell, (c) beam collimators, (d) cold baffle, (e) diffusion pumps, (f) magnet coil for ion removal, (g) titanium getter pumps, (h) transverse water-vapor beam, (i) fast-operating valve, (j) molybdenum getter pumps, (k) magnetic axis, (l) trapping chamber, (m) mirror field coils, (n) titanium targets.

The processes expected to control the trapping are gas-collisional ionization of beam atoms and Lorentz-force ionization of excited beam atoms. In the absence of cooperative effects, charge transfer between residual gas molecules and trapped protons would be the dominant loss process. Other trapping and loss mechanisms have been discussed[2] but can be neglected here. The spatially averaged trapped-ion density, $\bar{N}$, is then given by the approximate expression

$$\bar{N} = V^{-1}[Ln_0\sigma_{01} + f]I\tau_{cx}, \qquad (1)$$

where I is the injected beam flux (atoms/sec), τ_{cx} is the characteristic charge-exchange time, V is the plasma volume, L is the beam path length in the

[1] C. C. Damm, A. H. Futch, F. Gordon, A. L. Hunt, E. C. Popp, R. F. Post, and J. F. Steinhaus, Nucl. Fusion 1, 280 (1961).

[2] R. F. Post, in *Proceedings of the Fourth International Conference on Ionization Phenomena in Gases* (North-Holland Publishing Company, Amsterdam, 1960), Vol. II, p. 987.

plasma, n_0 is the residual gas density, σ_{01} is the ionization cross section, and f is the beam fraction ionized by the Lorentz force within the plasma volume.

In this description, the plasma is expected to be azimuthally uniform since the trapped ions precess about the magnetic axis of the cylindrically symmetric field by reason of a ∇B drift. The precession period ranges from about 20 to 100 μsec which is short compared with the characteristic buildup time of about 100 msec determined by τ_{cx}. The radial distribution of trapped ions is expected to be peaked on the magnetic axis in the pressure regime where gas trapping dominates.[3] In the region of $I\tau_{cx}$ where Lorentz-force trapping dominates, the radial distribution should be approximately uniform to within an orbit diameter of the wall. This is because the Lorentz trapping rate depends on the radial gradient of axial field component, $\partial B_z/\partial r$, which increases approximately linearly with radius in our field [see Sec. II, Eq. (2)]. The increase in trapping rate with radius is balanced by the linear increase with radius of the volume element through which the trapped ions precess. The axial extent of the plasma should be limited to the beam region in which trapping occurs since magnetic mirror forces inhibit axial excursions. Scattering collisions at the expected densities are negligible.

We would expect the plasma to be quasi-neutral since every ionizing event deposits both an ion and an electron within the plasma volume. The plasma potential with respect to the chamber wall is related to the electron temperature and should be less than 50 V because the energy transfer from hot ions to cold electrons is very slow at the expected density.[3]

Equation (1) predicts densities of about 10^8 ions/cm^3 for the operating conditions of the present experiment. Such densities are high enough (Debye length $= \lambda_D \approx 1$ cm $\ll$ plasma dimensions) to suggest that cooperative effects could be important, modifying the simple description of the plasma given above. We expect to observe a flute or drift instability[4] because of the negative field-gradient characteristic of the magnetic mirror field. In fact this type of instability is observed and apparently dominates the plasma behavior. The theory appropriate to our low density regime has been described by Mikhailovskii[5] and by Post[6] and yields the general features of the plasma as observed. A more recent treatment of the same problem by Kuo *et al.*,[7] which is extended in the present paper, describes this aspect of the plasma in some detail.

A second class of instability to be expected is the electrostatic resonance instability of the general type first proposed by Harris.[8] Such instabilities may occur in the presence of velocity space anisotropy of the plasma or in plasmas with peaked ion-energy distributions whenever the electron plasma frequency exceeds a critical value. The approximate critical condition is that the plasma frequency, ω_{pe}, exceeds the ion gyrofrequency, ω_{ci}. This type of instability is also observed, but a detailed comparison with theory is not yet possible.

II. APPARATUS AND OPERATING PARAMETERS

As in any energetic-particle injection experiment where one attempts to build the plasma density by accumulation of trapped ions, the product of beam intensity and characteristic charge-exchange loss time must be maximized if useful plasma densities are to be achieved. The design of the present beam line and vacuum system is an attempt to maximize this product. The experimental arrangement is shown schematically in Fig. 1 and described below.

The magnetic mirror field is formed by a pair of copper coils of 40-cm i.d. cooled with liquid nitrogen for economy of power. The mirror ratio, defined as the ratio of maximum field intensity to midplane field intensity (both measured on axis), is 1.34 and the mirror spacing is 63 cm. The axial component of field intensity within the useful region is given approximately by the expression

$$B_z = B_0\left[\frac{1 - 0.145(1 + 0.0025r^2)\cos(0.10z)}{1 - 0.145}\right], \qquad -31.4 \le z \le 31.4, \quad 0 \le r \le 12, \qquad (2)$$

where B_0 is the midplane field intensity on axis and z and r are in centimeters. Field pulses are usually of several seconds duration, and at the highest fields used ($B_0 \approx 30$ kG), the field intensity is constant within 5% for 5 sec. This time is more than sufficient to establish the plasma configuration. The time required for recooling the coils results in an injection cycle time of about 5 min.

Details of the ion source and beam formation have been described elsewhere.[9] The 20-keV protons

[3] A. H. Futch, Jr., W. Heckrotte, C. C. Damm, J. Killeen, and L. E. Mish, Phys. Fluids **5**, 1277 (1962).
[4] M. N. Rosenbluth and C. L. Longmire, Ann. Phys. (N. Y.) **1**, 120 (1957).
[5] A. B. Mikhailovskii, Zh. Eksperim. i Teor. Fiz. **43**, 509 (1962) [English transl.: Soviet Phys.—JETP **16**, 364 (1963)].
[6] R. F. Post, Bull. Am. Phys. Soc. **8**, 166 (1963).
[7] L. G. Kuo, E. G. Murphy, M. Petravic, and D. R. Sweetman, Phys. Fluids **7**, 988 (1964).
[8] E. G. Harris, Phys. Rev. Letters **2**, 34 (1959).
[9] F. J. Gordon and C. C. Damm, Rev. Sci. Instr. **34**, 963 (1963).

are neutralized by the charge-exchange process in a combination of hydrogen and nitrogen gas diffusing along the beam tube from the ion source region. Enough water vapor is added to the neutralizing cell to optimize the atomic beam. The total pressure in the neutralizing region is usually about 10^{-3} Torr.

The hydrogen atom beam is injected diametrically across the midplane of the mirror field for controlled periods of up to several seconds during the magnetic field pulse. It is possible to switch the beam on or off rapidly by variation of the 20-kV accelerating potential on the ion source. The beam intensity is adjustable to 45 mA (power equivalent). The beam cross section is defined by a pair of 2.0 × 5.1-cm rectangular collimating apertures. The first of these is located at the downstream end of the neutralizing cell, 385 cm from the magnetic field axis, while the second is 121 cm from the axis. This results in a maximum beam size of 3.8 × 9.8 cm within the trapping region with the larger dimension along the axial direction. The most intense portion of the beam is within this maximum dimension and the full size at half-maximum intensity is estimated to be 3.0 × 8.0 cm. The average beam flux is thus about 1.1×10^{16} atoms/cm^2 sec at maximum beam intensity.

In order to minimize plasma losses due to charge transfer, the neutral gas density in the plasma region must be minimized. The differential pumping system between the neutralizer and the trapping region greatly reduces the flow of gas to the trapping chamber. It consists of six stages. A cold baffle just downstream from the neutralizer removes most of the water vapor. Beyond this, a pair of trapped 6-in. oil diffusion pumps (speed $\approx$ 2400 liters/sec for hydrogen) reduces the gauge pressure to 2×10^{-5} Torr (gauges are calibrated for nitrogen). This pressure level includes the contribution of the residual charged components (H^+ and H^-) which constitute about 20% of the total beam and which are separated at this point by a local magnetic field. Two stages of evaporated-titanium getter pumping follow with low conductance tubes (just larger than beam size) joining each pumping stage to the next. A movable beam target in the first of these pumps is used for focusing and monitoring the continuous beam until the time of injection. Between the titanium pumps and the trapping region are two stages of fast molybdenum-getter pumping as described by Hunt *et al.*[10] Except during the injection period, these pumps are isolated from the higher pressure regions and from the beam by a fast-operating valve. During injection the gauge pressure in the second molybdenum pump is about 5×10^{-9} Torr.

The untrapped beam leaves the mirror field region through a close-fitting tube and terminates on a liquid-nitrogen-cooled titanium target at 560 cm from the mirror field axis. Surrounding the termination target, a large titanium getter pump maintains a gauge pressure of less than 10^{-8} Torr under full beam load. Between this pump and the trapping chamber two additional molybdenum getter pumps operate in the 10^{-9} Torr range and reduce the diffusion of gas from the beam disposal pump back to the trapping chamber.

The trapping chamber itself contains a liquid-nitrogen-cooled liner and is evacuated by two trapped 6-in. oil diffusion pumps. After a moderate bakeout (to $\sim$ 100° C), the chamber is cooled and molybdenum is evaporated onto as much of the inner surface as possible from filaments located outside the plasma region (Fig. 2). Very high pumping speeds are obtained in this way,[11] and the base pressure achieved is usually $1\text{–}3 \times 10^{-10}$ Torr (gauge).

During beam injection the local gas density in the trapping region increases by an amount equivalent to about 10^{-11} Torr (gauge)/mA, probably due to a very small fraction of the beam striking the edges of the beam tube. The local density measurements are made by positioning an ionization gauge (Fig. 2) just above the beam, near the magnetic axis, but without magnetic field. An ionization gauge located at the end of a long pipe (Fig. 2) registers a pressure rise of only about 30% of the central gauge rise, emphasizing the local nature of the gas density increase. This remote gauge is magnetically shielded and operates independently of the mirror field intensity.

Some additional pressure rise is expected with magnetic field because of excited beam atoms ionizing by Lorentz-force breakup in the fringe field region. This beam fraction can be estimated from measurements made in another experiment[12] and is of the order of 10^{-3} at 25 kG. The gas contribution from this source has not been measured directly but has been estimated to be small from the observed plasma charge-exchange rate.

Within the beam volume the gas density is also increased by molecular streaming from the neutralizer. By means of the movable ionization gauge this

[10] A. L. Hunt, C. C. Damm, and E. C. Popp, J. Appl. Phys. **32**, 1937 (1961).

[11] A. L. Hunt, C. C. Damm, and E. C. Popp, in *Advances in Cryogenic Engineering*, edited by K. Timmerhaus (Plenum Press, New York, 1963), Vol. 8, p. 110.

[12] A. H. Futch, Jr. and C. C. Damm, Nucl. Fusion **3**, 124 (1963).

streaming has been measured directly and is equivalent to 7×10^{-10} Torr H_2 at a neutralizer pressure of 2.6×10^{-4} Torr. A molecular beam of water vapor crossing the atomic beam line near the first titanium pump reduces the streaming density by a factor of 3, to 2.5×10^{-10} Torr H_2, by inducing small-angle scattering of the molecular beam from the neutralizer. The water-vapor scattering beam was not used for most of the measurements described here.

Including the base pressure, the pressure rise due to the beam, and the molecular streaming (but neglecting the unmeasured Lorentz ionization contribution), the neutral gas density on the magnetic axis with a 45-mA beam is estimated to be equivalent to about 2×10^{-9} Torr H_2. Since the molecular streaming is localized, the chamber pressure averaged over the plasma volume is estimated to be about 1.5×10^{-9} Torr H_2, leading to a characteristic charge-exchange time of 170 msec for 20-keV protons. When required, the gas pressure can be increased by admitting helium to the chamber through a controllable leak valve.

The plasma radius is limited by an adjustable copper plate, called the "radial limiter" in Fig. 2. Most of the measurements are made with the radial limiter set at $r = 12$ cm.

III. DIAGNOSTIC METHODS

A. Density Profile

The trapped fast-ion density as a function of radius and azimuth is investigated with the "radial profile detector." This detector collects charged particles escaping through one of the mirrors. In particular, it detects slow ions resulting from charge-exchange collisions of the trapped protons with the background gas. Because the rate of these charge-exchange collisions in the plasma is proportional to the trapped ion density and the background gas density, the resulting slow-ion distribution is related to the trapped ion distribution. With the assumption that the slow ion distribution is maintained as these ions are promptly accelerated by the positive plasma potential along magnetic field lines and out of the plasma region, the variations in the flux of these escaping ions are related to the spatial variations of the trapped ion density. To make this relation quantitative, certain additional assumptions are required. The background gas density is assumed uniform except in the region of the beam where it is higher due to molecular streaming. We consider that the ions collected by the radial profile detector are predominantly from charge-exchange

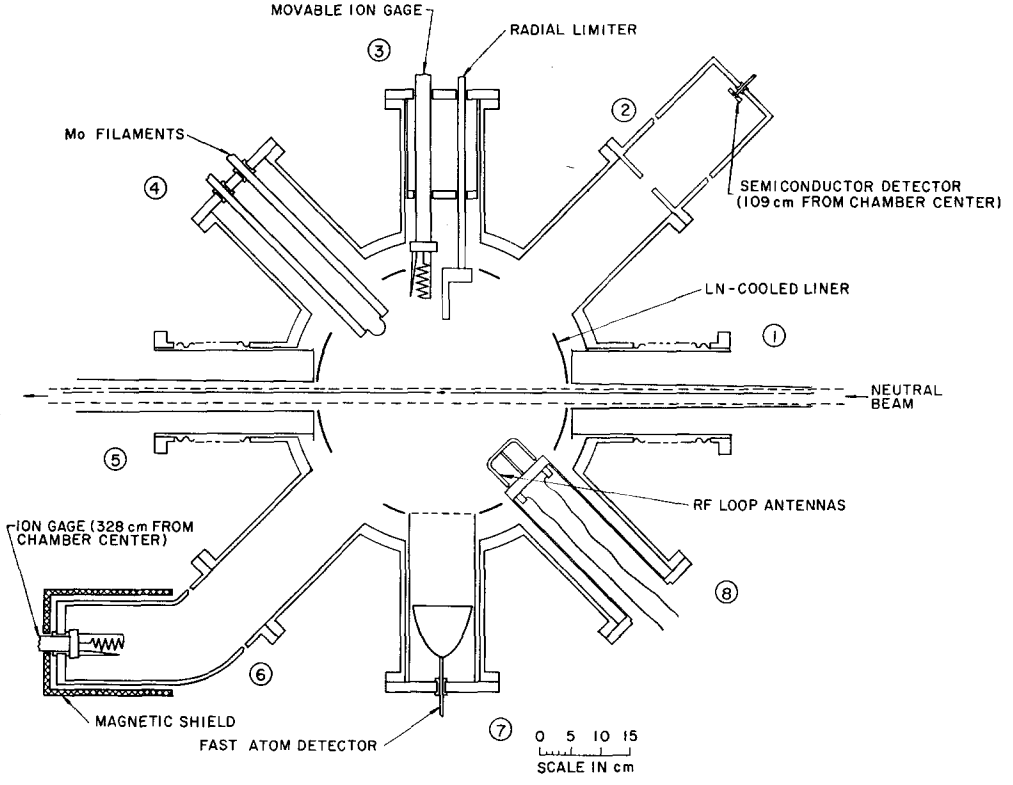

FIG. 2. Schematic drawing of trapping chamber, looking along mirror field axis.

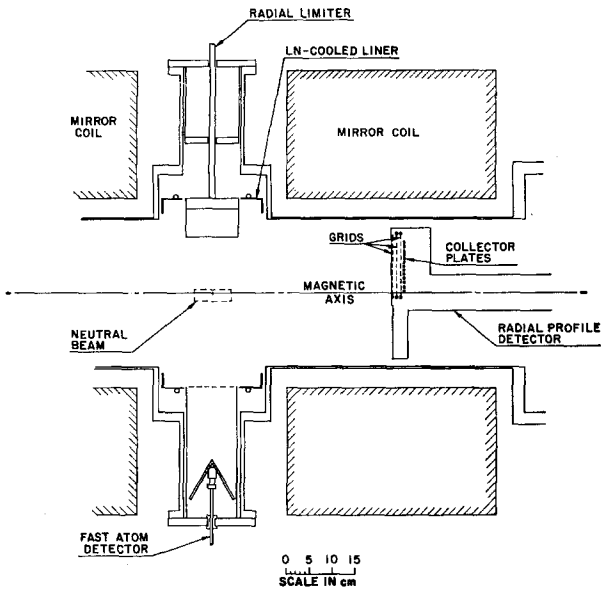

FIG. 3. Schematic drawing of trapping chamber region, looking along beam line.

reactions. There is also a smaller contribution from ionization of the background gas by trapped ions and electrons. In addition, we observe a signal from the beam region which is evidently due to ionization caused by the interaction of the beam with the background gas and which is negligible with the usual conditions of good vacuum. Finally, an assumption concerning the axial extent of the plasma is required since the signal current measures only the line density of charge.

The main features of the profile detector are shown in Fig. 3. Seventeen detector plates are uniformly positioned along a radial line between $r = 0$ (magnetic axis) and $r = 11$ cm. Each plate extends about 0.5 cm radially and is 1 cm^2 in area. Through use of two sets of sliding vacuum seals with differential pumping between, the detectors can be rotated to any desired azimuthal position. The axial position is also adjustable, and the detectors are usually located just outside of one mirror.

There are three high-transmission tungsten grids in front of the collector plates. The wires comprising a grid cover about 6% of the area of the grid. The outer grid is permanently grounded, and the inner grid is usually biased negative with respect to the plates so as to suppress secondary electron emission from the plates. As a result of these precautions, secondary electron effects appear to be relatively unimportant in the profile measurements. The negative bias on the inner grid also prevents electrons escaping through the mirror from reaching the collector plates. We sometimes apply to the middle grid a variable positive bias in order to determine the energy distribution of the incident ions.

The ion currents collected by the 17 plates are usually time-averaged. These currents (10^{-10} to 10^{-9} A in magnitude) charge condensers, which are then read out and discharged by a sampling switch every 0.1 sec. The output of the sampling switch is amplified and recorded on an oscillograph as a radial profile. In this way, we can conveniently examine the magnitude, radial shape, and slow time variations of the ions escaping through the mirror.

We also can observe the effect of the 10- to 50-kc/sec plasma rotation and obtain some measure of the azimuthal distribution of the trapped ions by observing fast time variations in the collector currents. The currents from alternate collectors are amplified directly by fast low-current amplifiers of the type described by Bell *et al.*,[13] and the signals are displayed on several dual-beam oscilloscopes.

B. Average Density of Fast Ions

The average fast-ion density is measured in three ways. The first two of these measures the flux of fast atoms observed at the periphery of the trapping region, these atoms being the result of charge-exchange collisions of plasma protons with background gas molecules. While this flux is proportional to the product of fast ion density and gas density, the integrated flux arriving at the detector after turn-off of the injected beam is independent of gas density, thus providing an "absolute" method of determining plasma density. In using the method we assume that charge-exchange collision is the only appreciable loss mechanism during plasma decay, an assumption supported by the comparison of measured decay rates and calculated rates based on gas pressure measurements. We also assume that the emission of fast atoms is azimuthally symmetric when time-averaged over the plasma rotation period. With these assumptions, the average density of ions in the plasma at the time of beam turn-off, t_0, is given by

$$\bar{N} = (G\delta V')^{-1} \int_{t_0}^{\infty} i\, dt, \tag{3}$$

where $\bar{N}$ is the average ion density within the plasma volume V' seen by the detector, i is the observed detector current (particles/sec), G is a solid angle factor, and δ is the detector efficiency.

In the first method of observing the trapped ion

[13] P. R. Bell *et al.*, in Oak Ridge Thermonuclear Division Report, ORNL-3472 (1963), p. 22.

density, we monitor the secondary electrons emitted by fast neutrals incident upon our "fast atom detector." This large-aperture detector (Fig. 3) looks at the entire plasma volume with reasonably uniform sensitivity. The emission of electrons by ultraviolet radiation is estimated to be small compared with the emission by the fast atoms and has been neglected. With usual operating conditions, the plasma volume is 3.6 liters and G is estimated to be 0.03. The major uncertainty lies in the value of δ, the secondary electron coefficient, which depends on the condition of the detector surface. From the work of Large and Whitlock,[14] from a consideration of the particle angle of incidence and the surface roughness, and from a knowledge of the fraction of our detector coated with clean molybdenum, we estimate $\delta = 2$. The uncertainty in this factor may be as high as a factor of 2. However, an additional calibration has been obtained in the pressure regime where gas trapping is predominant [see Eq. (1)]. There the trapped ion density is independent of gas density (since τ_{ex} is inversely proportional to the gas density) and can be calculated readily from the measured beam intensity. The agreement with the measured density using $\delta = 2$ is satisfactory (see below).

The required integration of detector current is normally accomplished electronically, so that an immediate density readout is obtained at the end of each pulse.

During steady beam injection we believe the gas density in the plasma region to be constant in time. Hence, regardless of absolute calibration, the variation of the fast atom detector's signal reflects variation in fast ion density.

The second detector of fast atoms makes use of a semiconductor element (Ortec silicon surface-barrier detector) to count individual atoms, thus eliminating the uncertainty of secondary electron emission. By minimizing stray capacitance in the leads and cooling the detector, the pulse height spectrum of 20-keV protons is well resolved from the noise and, with proper discriminator bias, δ is essentially unity. In this case, however, the volume of plasma observed is a thin slab 2.5 cm in width extending across the plasma diameter. The volume, V', and the solid angle factor, G, are adjusted by controlling the aperture in front of the solid state element to give a suitable counting rate. Apertures are generally 0.005 to 0.020 cm in diameter. The semiconductor detector is located as shown in Fig. 2.

The third method of fast-ion density measurement also makes use of the products of charge exchange. While the fast atom detector and the semiconductor detector monitor the fast neutrals, the radial profile detector collects the resulting slow ions that are ejected through one mirror. Because this detector is azimuthally selective and because the neutral gas density is not azimuthally uniform, it is necessary to rotate the detector between injection periods and obtain radial profiles at various azimuths. Then, from the composite profile and the average chamber pressure, we arrive at a time-averaged radial density distribution. We integrate this distribution over radius and azimuth to obtain the total number of trapped ions, and hence, the average density (neglecting possible axial spreading).

For a certain set of operating conditions, a comparison of the three methods of fast-ion density measurement yielded the following results: fast atom detector, $1.9 \times 10^7/\text{cm}^3$; semiconductor detector, $1.8 \times 10^7/\text{cm}^3$; and profile detector, $1.5 \times 10^7/\text{cm}^3$. Use of the gas trapping calibration for the fast atom detector instead of $\delta = 2$ lowers the first value to $1.8 \times 10^7/\text{cm}^3$. The agreement among these measurements is better than one would expect considering the various uncertainties that enter into these results. Normally we will quote the value of average density obtained from the fast atom detector.

C. Average Electron Density

Some indications of the electron density, N_e, of the plasma are obtained from measurements of the phase shift of a 9006-Mc/sec beam that is transmitted through the plasma. Measurements of phase shifts less than 50 μrad are accomplished by use of synchronous detection and a null type of bridge measurement described in more detail elsewhere.[15]

The microwave signal traverses the plasma twice, returning to the radiating horn from a focusing reflector located at the opposite wall of the chamber. About 70% of the power radiated from the horn is returned directly from the reflector. The principal source of "noise" in the measurement is attributed to changes in position of the various reflecting surfaces within the vacuum chamber. In spite of these spurious reflections, the use of a measured movement of the focusing reflector is considered to be a valid direct calibration of phase shift for the over-all system. In making the calibration the beam is treated as a plane wave and the plasma as a plane slab 24 cm thick. Thus, no attempt is made to correct for the

[14] L. N. Large and W. S. Whitlock, Proc. Phys. Soc. **79**, 148 (1962).

[15] A. L. Gardner (to be published).

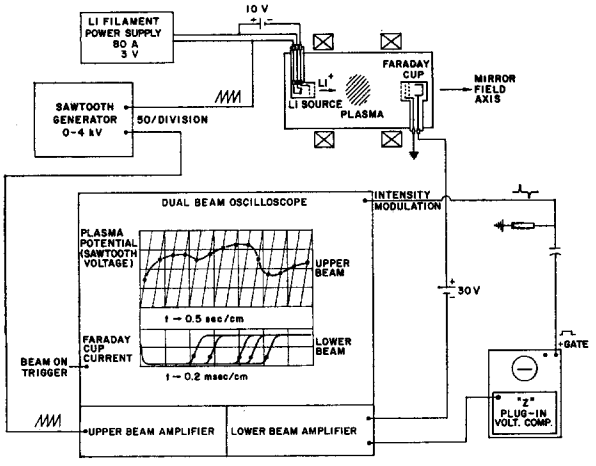

FIG. 4. Schematic diagram of the Li^+ beam apparatus used to measure the plasma potential. The method of displaying the plasma potential versus time is illustrated.

divergence of the microwave beam or the radial distribution of the electrons.

To improve the signal-to-noise ratio, the fast atom beam feeding the plasma is chopped (for these measurements only) with 50% duty ratio at a rate of 20 or 60/7 cps and the phase shift response is synchronously detected. The plasma buildup time is shorter than the chopping half-period, but in order to achieve significant plasma decay during 1/40 sec, a background gas of helium at 2.7×10^{-7} Torr is used. The sensing of the microwave response is made over a 5-msec period ending about 0.5 msec before the end of the chopping half-cycle. Thus, the microwave phase shift corresponds to the change in N_e between the turn-off time of the fast atom beam and an average time of either 22 or 55 msec later.

In practice the (gated) output from the synchronous detector is integrated and the quantity measured is the change in slope of the integrated signals as the phase of the fast atom-beam chopping is changed by 180° with nothing else changed. Since the phase of the synchronous detector is not altered, the change of slope produced by the phase reversal is twice as large as that experienced at initial turn-on or at final turn-off of the chopped beam.

D. Plasma Potential

The method for measuring and recording the plasma potential to be described here is basically an extension of the lithium-ion beam technique which has been described by Haste and Barnett.[16] Only a brief description of the technique will be given here as additional details may be obtained from a previous paper.[17]

Figure 4 is a schematic diagram showing the method and equipment used. The plasma chamber is represented at the top of the diagram by the large rectangle. The lithium ion source, placed at one end of the machine, consists of a tantalum filament coated with a lithium mineral, β eucryptite. Heating the filament to a dull red heat produces lithium ion (Li^+) emission, and a high voltage applied between the filament and a grounded screen accelerates the ions to the desired energy.

If the lithium ion energy is greater than the (retarding) plasma potential, the lithium ions will follow the magnetic field lines through the plasma to be detected by a Faraday cup at the opposite end of the machine. The accelerating potential at which transmission through the plasma occurs is defined as the plasma potential.

The usual method of operation is to apply a repetitive sawtooth accelerating voltage to the Li^+ source and observe the point at which transmission commences for each sweep of the sawtooth voltage. An electronic method employing two oscilloscopes is used for displaying the plasma potential as a function of time. The interconnections of the two scopes are shown in Fig. 4. The Li^+ current collected by the Faraday cup is fed to the vertical deflection amplifier of the lower beam of a dual-beam oscilloscope and to a voltage comparator preamplifier of a second oscilloscope. When transmission occurs the ion current triggers the sweep of the second oscilloscope through the voltage comparator circuit. The positive gate out (a few microseconds long) then passes through a differentiating circuit, and the trailing negative pulse is used to intensity-modulate both beams of the first oscilloscope. The sawtooth voltage is fed into the upper beam of this oscilloscope producing a vertical raster display which is brightened at the voltage corresponding to transmission of the lithium ion beam.

A schematic diagram of the oscilloscope traces observed is included in Fig. 4. The lower beam trace shows a number of possible curves produced by the current to the Faraday cup, each curve corresponding to a single sweep of the sawtooth voltage. The upper beam trace illustrates the manner in which the time dependence of the plasma potential is displayed. The locus of brightened points shows the variation of plasma potential during a period of several seconds. The time resolution corresponds to

[16] G. R. Haste and C. F. Barnett, Bull. Am. Phys. Soc. 7, 152 (1962).

[17] A. F. Waugh and A. H. Futch, Jr., IEEE Trans. Nucl. Sci. NS-11, 221 (1964).

the sawtooth repetition rate and is about 1 msec at best.

An independent method of measuring the plasma potential utilizes the gridded Faraday cup alone. Slow ions formed in the plasma by ionization of the background gas and by charge-exchange collisions are expelled from the plasma and arrive at a grounded detector with an axial energy approximately equal to the plasma potential. The measurement is obtained by increasing the positive bias on the center grid and noting the voltage at which ion collection ceases. The outer and inner grids are grounded to prevent the biasing voltage from disturbing either the plasma or the emission of secondary electrons from the collector cup. The secondary electron emission is suppressed by a small positive bias on the cup. Plasma potential measurements obtained by this method agree with values obtained by the Li^+ transmission technique.

E. Radio-Frequency Measurements

Radio-frequency signals, particularly near the ion gyrofrequency, ω_{ci}, are detected by two pairs of loop antennas oriented in two perpendicular planes. A balanced electrostatic shield is employed to achieve cancellation of the effects of currents induced by radial electric fields. The construction of one pair of loops is shown schematically in Fig. 5. The loops are located in the midplane region just beyond the outer radius of the plasma (Fig. 2). One pair of antenna loops is oriented for maximum sensitivity to the axial rf magnetic-field component, H_z, and the other is oriented for maximum sensitivity to the azimuthal component, H_θ.

The signals from each pair of loops are amplified differentially to complete cancellation of electrostatic components. The amplified signal is then displayed directly on an oscilloscope and can also be analyzed in a spectrum analyzer. The analyzer used (Pentrix Model L-20) is capable of a 1-kc sweep rate with an adjustable frequency sweep range. A mechanical "chopper" switch running at 120 cps permits analysis and display of the two rf components alternately. A raster-type oscilloscope display, driven by the spectrum-analyzer sweeping voltage with the spot intensified by the amplitude of the analyzed signal, gives us a record of the frequency and intensity of both components of the rf signal, H_z and H_θ, versus time.

IV. OBSERVATIONS AND RESULTS

We describe the spatial distribution of the trapped ions, the average density of ions and electrons,

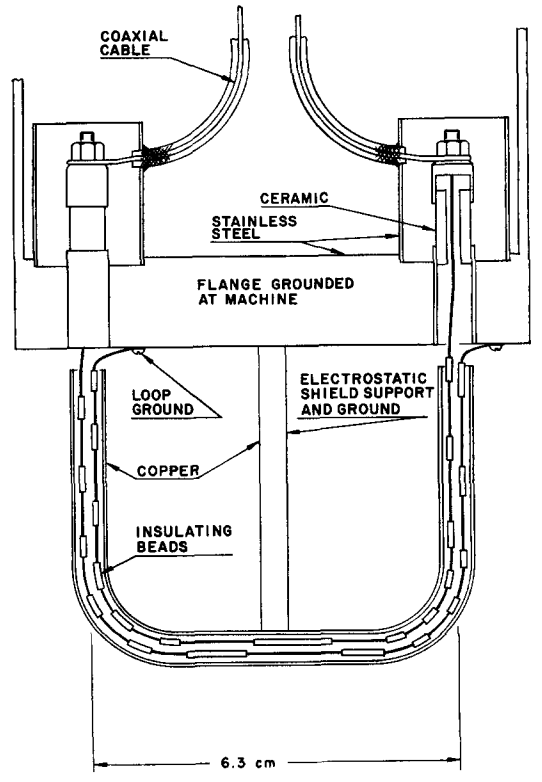

FIG. 5. Loop antennas used for detecting rf signals. Not shown is the set of two loops perpendicular to the plane of the drawing.

and the plasma potential, relating the plasma characteristics to the low-density flute theory whenever possible. It is seen that the plasma behavior is generally understandable in terms of this theory although of course a linear theory cannot describe the actual plasma in all detail. The interrelated effects of oscillations at the ion gyrofrequency also considerably complicate the detailed description.

A. Spatial Distribution

Two different plasma configurations are actually observed, both having nonuniform radial and azimuthal distributions. These configurations are determined from the radial-profile detector signals and typical examples are shown in Fig. 6. The case recorded there depicts a configuration change during a single injection period at a central magnetic field of 21 kG. One distribution is characterized by a peak profile-detector signal on the magnetic axis ("centered" distribution). The second yields a low current near the axis and a peak signal at intermediate radii ("off-center" distribution). The currents shown are time-averaged over a 0.1-sec interval. In the figure insert, we show the fast-atom detector signal for this case which is seen to decrease

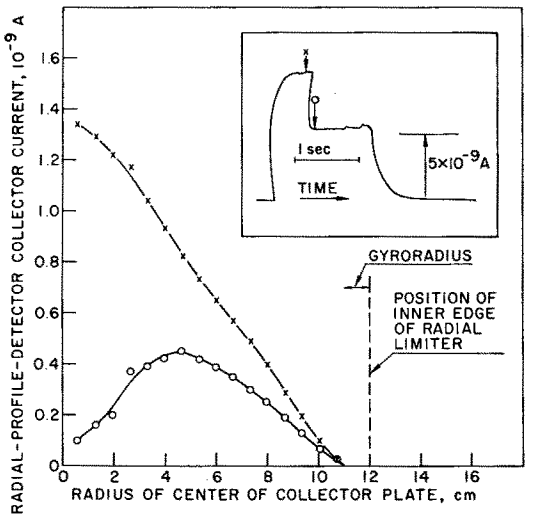

FIG. 6. Radial profile of the plasma before (×) and after (⊙) a major decrease in the fast-atom detector signal. The radius scale has been transformed along magnetic field lines from the radial-profile detector position to the median plane. The insert shows the fast-atom detector signal for the entire injection period; arrows indicate the points at which the profiles were measured.

when the configuration change occurs. The simultaneous shifts in the other detector signals will be discussed later. With the radial limiter set at $r = 12$ cm, configuration changes in either direction may occur at random or may be triggered, for instance by a spark in the ion source. With the radial limiter moved to smaller radii, the centered distribution is always observed.

When we examine the profile detector signals with fast electronics, we find that the ion currents arriving at the collectors are intensity-modulated in time. This modulation indicates that the plasma is not spread uniformly around the magnetic axis but instead is clumped azimuthally and is rotating about the axis. The clumping and rotation is observed for both the centered and off-center configurations. The frequency of rotation corresponds to the low frequency (10–50-kc/sec) oscillations detected by the radial limiter and reported in an earlier paper.[18] In that paper the oscillations were identified with the $m = 1$ mode of low-density flute oscillation described by Mikhailovskii[5] and by Post.[6]

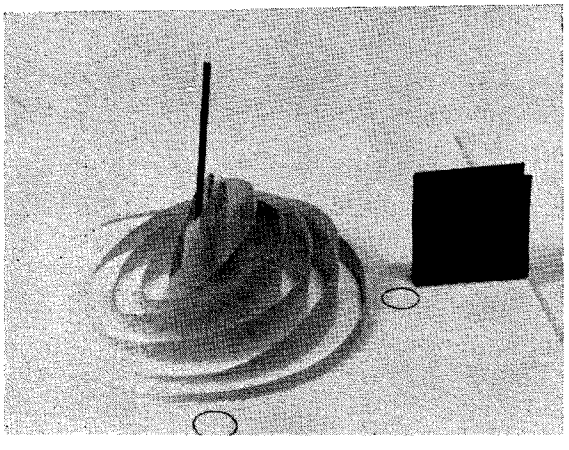

FIG. 7. Photograph of model showing centered plasma distribution. Depicted are the magnetic axis, radial limiter (at the right), and the trapped proton orbit size.

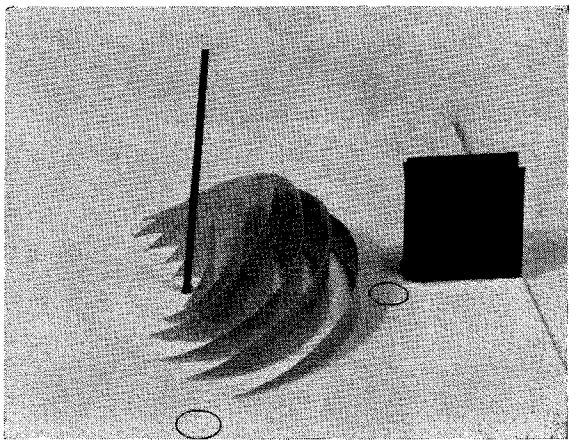

FIG. 8. Photograph of model showing off-center plasma distribution.

Figures 7 and 8 are photographs of models of the two plasma configurations based on the modulated profile-detector signals. Each semicircular or circular section represents the time variation of the ion current arriving at one of the collector plates. These time variations have been transformed in the models to azimuthal variations at a particular instant of time. Again evident is the difference in the radial position of the peak signals in the two configurations. The peak collector currents in the two examples are about equal, a fact not evident from Fig. 6, the time-averaged case, because the effect of the azimuthal clumping is not indicated. One apparent difference in the two models is the azimuthal extent of the plasma which is greater in the centered case than in the off-center case. Because the models include the electronic time resolution, the actual plasma masses probably have about two-thirds the azimuthal extent shown by the models. The peaks of the signals from the various collectors appear to be in phase azimuthally.

To interpret the models in Figs. 7 and 8 in terms of trapped-ion density distributions, we need information on the plasma distribution and extent along the direction of the magnetic axis. This in-

[18] C. C. Damm, J. H. Foote, A. H. Futch, Jr., and R. F. Post, Phys. Rev. Letters 10, 323 (1963).

formation is necessary because the ions contributing to the profile detector signals originate over a range of axial positions, presumably from the midplane to the edge of the plasma nearest the detector. We assume the axial extent of the plasma to be at least the width of the beam which extends to about 4 cm on each side of the midplane, because trapping can occur throughout this region. Axial spreading beyond the beam region is indicated by an off-midplane fast-atom detector which observes a volume located between 8 and 10 cm from the midplane. It detects a small amount of plasma there in the centered configuration but essentially no plasma in the off-center case. Although we can detect axial spreading, we cannot say how the spreading varies with radius. We have made approximate calculations of possible plasma spreading caused by the large positive plasma potential which is observed (see Sec. IVB). Our observations, coupled with these calculations, lead us to expect the model of Fig. 8 to be approximately correct for the density distribution in the off-center case, but the model of Fig. 7 is expected to require some correction in order to represent the centered density distribution near the midplane. We believe that the primary features of a rotating, nonuniform plasma mass are firmly established, however, regardless of the details of axial spreading. The ion distribution is certainly far different from that predicted when cooperative effects are neglected.

It should be noted that we are discussing the regime of full beam, good vacuum, and high magnetic field (21 kG). As the beam is decreased or as the pressure is increased, both the plasma potential and the axial spreading are observed to decrease. The shape of the time-averaged radial profile for the centered distribution remains approximately constant as the pressure is increased. The off-center distribution is not observed at high pressure or low beam. Both radial distributions continue to be seen as the magnetic field is lowered to about 12 kG, at which point the effects of large gyroradius apparently begin to erase the distinctive features, creating a distribution which is more nearly uniform with radius.

B. Ion Density and Plasma Potential

The measured average trapped-ion densities fall into two groups characterized by the two density distributions just described. The points obtained at a central magnetic field of 21 kG are plotted in Fig. 9 for comparison with the value expected on the basis of Eq. (1). In calculating $\bar{N}$ from Eq. (1),

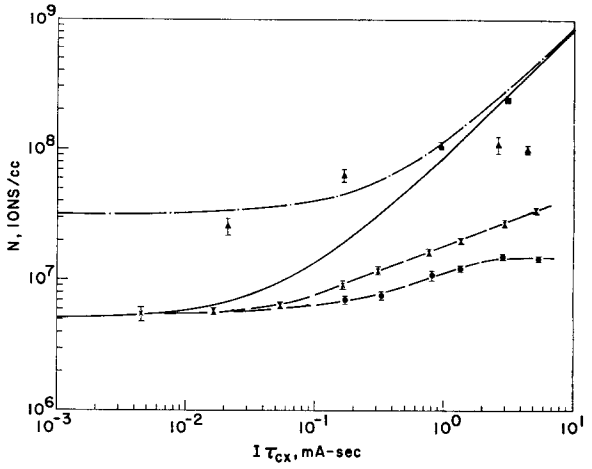

FIG. 9. Trapped-ion density versus the product of beam level and charge-exchange time. $I = 36$ mA for all $I\tau_{cx} < 0.2$ mA sec. Solid and dot-dash curves represent theoretical average density and peak density behavior, respectively, if one assumes charge-exchange loss only and no collective effects. Experimental measurements: circles, off-center distribution, average density; crosses, centered distribution, average density; triangles, centered distribution, peak density; square, centered distribution, peak density (13-cm plasma diam instead of the usual 24-cm diam). Errors are standard deviation of the mean.

the following values are used: $L = 24$ cm, $V = 3.6$ liters, $v = 2.0 \times 10^8$ cm/sec, $\sigma_{01} = 1.35 \times 10^{-16}$ cm^2 and $\sigma_{10} = 1.92 \times 10^{-16}$ cm^2, $f = 5.0 \times 10^{-5}$. The charge-exchange and ionization cross sections for helium[19] are used in the high-pressure, gas-trapping regime where the gas is predominantly helium. The value of f is obtained from measured excited-state populations[12] and involves an estimate of Stark lifetimes for decay of the excited states.[20] For simplicity of comparison, the beam current is maintained constant (at 36 mA) for all $I\tau_{cx}$ values below 0.2 mA sec, both experimentally and in the calculation of $\bar{N}$. Above this value of $I\tau_{cx}$, both beam and gas density are varied.

The off-center configuration exhibits a definite density limit at 1.5×10^7 ions/cm^3, as $I\tau_{cx}$ is increased above the gas trapping region. The centered configuration has a higher average density and apparently continues to increase with $I\tau_{cx}$. However, the increase is much less than linear, and the absolute value of the density is an order of magnitude below the expected value at the highest $I\tau_{cx}$.

Ion losses in addition to charge exchange are evident for both configurations. We identify these losses with the onset of unstable flute oscillations at a density which can be predicted quantitatively from

[19] S. K. Allison, Rev. Mod. Phys. **30**, 1137 (1958).
[20] J. R. Hiskes, C. B. Tarter, and D. A. Moody, Phys. Rev. **133**, A424 (1964).

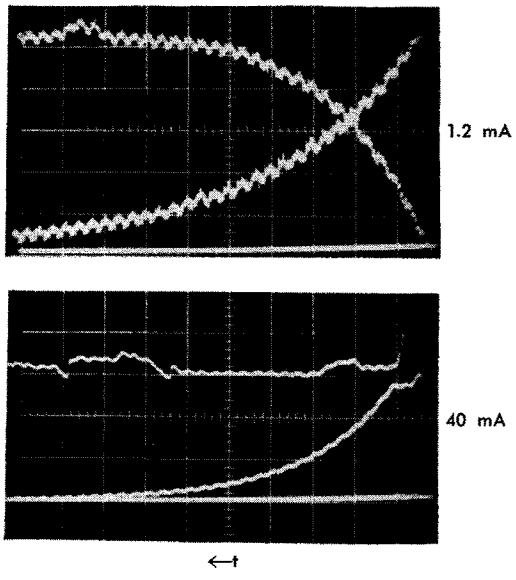

FIG. 10. Superimposed oscilloscope traces of the fast-atom detector signals during plasma buildup and decay at two levels of injected beam. Horizontal scale = 50 msec/div.

the theory of Kuo *et al.*[7] This theoretical treatment was developed in connection with the Culham Phoenix experiment, where a similar density limitation is seen, and represents an extension of the work of Mikhailovskii and Post. For our parameters the Kuo theory predicts the observed density limit within a factor of 2 which is remarkably good agreement.

The density limitation is evident from the fast-atom detector signal during plasma buildup. In Fig. 10 we have superimposed the buildup and decay signals at two different levels of injected beams. At the low beam current of 1.2 mA, both buildup and decay appear to be exponential, governed approximately by the charge-exchange loss rate. When the injected beam is increased to 40 mA, the density reaches its unstable limit, which is far below the value expected from Eq. (1), within 50 msec after the start of injection. At beam turn-off, the fast-atom detector signal drops by about 25% and then remains nearly constant for about 30 msec. This may be evidence that those ions spread axially outside the fast-atom detector field of view are collapsing toward the midplane after beam turn-off. (The contribution of these ions to the integrated signal is less than 25% and has been accounted for where necessary in Fig. 9.) The ensuing decay, however, is exponential with a characteristic time very close to the estimated charge-exchange time since the plasma is again below the unstable limit.

An explanation of the different density limits for the two plasma configurations was developed by relating observations of the plasma potential to an extension of the Kuo calculations. In the off-center configuration at high values of $I\tau_{cx}$, the measured plasma potential is typically 1–2 kV positive.[21] This is anomalously high since the classical energy transfer rate from hot ions to cold electrons is negligible. On this basis the plasma potential is expected to be less than 50 V. Present theories cannot yield the higher value observed, but qualitatively this value must derive from the self-consistent set of fields required for the fluting mode.

When the plasma changes to the centered configuration, not only does the average density increase but the plasma potential increases to +3–4 kV. The centered distribution is always accompanied by strong rf oscillations (at frequency ω_{ci} or $2\omega_{ci}$, polarized H_θ) and enhanced emission of electrons through the mirror region. The electron emission is observed on either the radial profile detector or the Faraday cup collector, properly biased. The rf activity is evidence of a velocity-space-type instability and is probably responsible for the electron emission, and hence, the increased plasma potential. An example of the simultaneous changes in some of the signals when the configuration changes is shown in Fig. 11.

At the measured density ($1–4 \times 10^7$ ions/cm^3) and with plasma potentials of the order of kilovolts, it is easy to verify that the ion and electron densities must be quite different.[21] The assumption of quasi-neutrality made by Kuo and co-workers must therefore be in question for our experiment. One of us (AHF) has extended the Kuo treatment to the case of unequal ion and electron densities, and this extension is shown in the Appendix. The resulting theory predicts an increase in the ion density at which the instability occurs as γ, the ratio of electron density to ion density, decreases. To compare theory and experiment, it is necessary to express the theoretical density limit as a function of the plasma potential instead of γ. The plasma

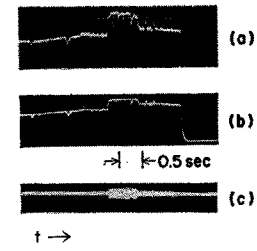

FIG. 11. Montage of oscilloscope traces showing correlated changes in (a) plasma potential, (b) average ion density, fast-atom detector signal, and (c) rf loop-antenna signal, H_θ polarization.

[21] A. H. Futch, Jr., Bull. Am. Phys. Soc. 9, 335 (1964).

potential is related to γ through the following solution for the potential of a cylindrical plasma column of length l:

$$\phi(r, z) = 4\pi e \sum_s \frac{J_0(\lambda_s r) N_0 (1 - \gamma)}{r_0^2 \lambda_s J_1^2(\lambda_s r_0)} \cdot \int_{-l/2}^{l/2} e^{-\lambda_s |z - z'|} \int_0^{r_0} \frac{N(r')}{N_0} J_0(\lambda_s r') r' \, dr' \, dz', \quad (4)$$

where N_0 is the ion density at $r = 0$ and the separation constants, λ_s, are determined by the condition that ϕ is zero at $r = r_0$. The radial distribution of the plasma, $N(r)/N_0$, is known from the profile detector measurements.

Using Eq. (4), the stability boundary derived in the Appendix (Fig. 15) may be replotted with the density at which the plasma becomes unstable as a function of the reciprocal of the plasma potential instead of γ. Since the experimental points are measurements of the average density over the plasma volume, the theoretical density distribution has been averaged over the volume for comparison with the experimental results. One then obtains the results shown in Fig. 12 where the smooth curve gives the theoretical results and the circled points are the experimental data.

Figure 13 shows a comparison of the experimental frequencies with which the plasma oscillates compared with the theoretical frequencies for the $m = 1$ mode as calculated from Eq. (A19) in the Appendix. Two theoretical curves are shown corresponding to values of γ equal to 1 and 0.5. The curve $\gamma = 1$ corresponds to results obtained previously by other workers[7] for equal ion and electron densities and for which there exists no zero order electric field. For this case one would expect to observe plasma frequencies of $\frac{1}{2}$ the gradient-B rotation frequency Ω_M, when the plasma density is limited by the instability. As shown in Fig. 12, when large plasma potentials are present, the critical density increases; the corresponding frequency at the critical density also increases since we now have an electric rotation due to the $\mathbf{E} \times \mathbf{B}$ drift of the zero order electric field which adds to the gradient-B rotation.

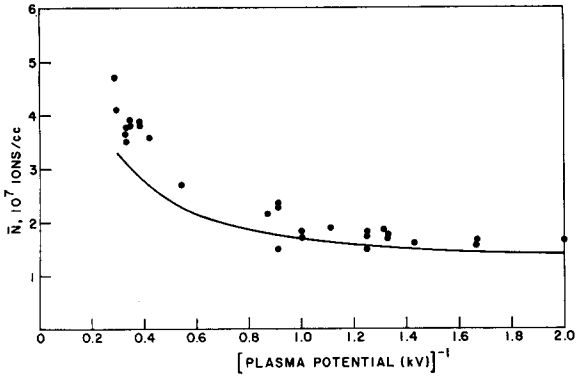

FIG. 12. Comparison of the experimental (circles) and theoretical (solid line) variation of average ion density at the unstable limit with the inverse of the plasma potential.

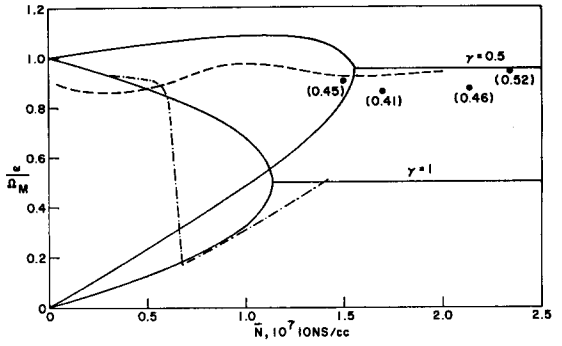

FIG. 13. Variation of the drift oscillation frequency with average ion density. The oscillation frequency, ω, is normalized to the ion precession frequency in the ∇B field, Ω_M. Theoretical curves (solid lines) are shown for two values of γ. Selected experimental curves, obtained during plasma decay, are dashed. Four experimental points obtained during beam injection are plotted with measured γ values in parenthesis.

Four experimental frequencies measured during beam injection are shown plotted in Fig. 13. Values of γ estimated from plasma potential measurements are shown in parenthesis. The frequencies observed agree quite well with what one expects when a plasma potential, and therefore, a zero order electric field is present. The two broken lines show examples of the frequency behavior of the plasma during the plasma decay following beam turn-off. Two different decay modes have been observed: one for which the frequency stays approximately constant as the density decreases and a second density-dependent mode for which the frequency decreases during the plasma decay. The density-dependent mode will sometimes change abruptly to the constant frequency mode as indicated in the figure. The constant frequency mode often persists to low densities during plasma decay. With particularly good vacuum, these oscillations have been observed for as long as 6 sec after beam turn-off, corresponding to a density decay by at least two orders of magnitude. A tentative explanation for the persistence of these coherent oscillations has been given by Furth,[22] who attributes the effects to dissipative mechansims in the plasma.

In Fig. 9 we have plotted peak ion densities (centered configuration) as determined by the profile detector, in addition to average density, for comparison with the peak density curve calculated from

[22] H. P. Furth, Bull. Am. Phys. Soc. **10**, 523 (1965).

an equation very similar to Eq. (1). This determination assumes no axial spreading outside of the beam region. The agreement is better than in the case of average density, particularly when the diameter of the plasma is decreased from 24 to 13 cm by moving the radial limiter. We conclude that on-axis particles are lost solely via charge exchange under some conditions, and this conclusion is independent of the question of axial spreading. The instability loss rate must therefore be a function of radius.

C. Average Electron Density

The measurement of electron density by the microwave phase-shift technique yields an independent estimate of the plasma density. Unfortunately, the necessity of admitting helium gas to shorten the plasma decay time precludes the possibility of a direct measurement of N_e in the high $I\tau_{cx}$ region where the plasma potential is changing. Ion and electron densities in the high pressure regime are expected to be nearly equal.

The results of a set of measurements give the following mean values for the decrease in electron density between the time of beam turn-off, $t = 0$, and either 0.022 or 0.055 sec later:

$$N_e(t = 0) - N_e(t = 0.022) = (1.2 \pm 0.1) \times 10^6/\text{cm}^3,$$

$$N_e(t = 0) - N_e(t = 0.055) = (2.7 \pm 0.3) \times 10^6/\text{cm}^3.$$

In order to obtain $N_e(t = 0)$ from these measurements, the characteristics of the electron density decay must be known. The decay of electron density in the plasma is complicated by various factors. Fast-atom detector measurements indicate that the density of energetic protons in the plasma decays exponentially with a time constant of about 6 msec at the selected gas pressure. The charge transfer process thus replaces the fast protons with slow helium ions in a comparable time. During beam injection the slow ions would be quickly discharged from the system because of the positive plasma potential, but in the decaying plasma this potential also falls at a rate similar to the fast-ion decay. Thus the remaining slow helium ions must eventually be scattered into the mirror loss cone by ion–ion collisions or collisions with the neutral helium. Furthermore, the slow ion energies and densities are in a regime where both types of scattering processes may be important. Since the electrons receive little additional heating in the decaying plasma, they cannot overcome any appreciable potential, and their decay is in turn governed by the loss rate of the slow ions.

In view of these complexities, one cannot hope to construct an accurate model for describing the electron density decay. However, in order to estimate $N_e(t = 0)$, calculations have been made for four simplified cases which are expected to bracket the actual situation. Two of these assume an exponential decay (starting at $t = 0$ or at $t = 6$ msec) and represent decays dominated by scattering on background gas, while the other two assume a decay proportional to N_e^2 (starting at $t = 0$ or $t = 6$ msec) and represent decays governed by Coulomb collisions. From these calculations, it appears likely that the actual average value of electron density for these conditions is bracketed by the extreme values of 3.9×10^6 and 1.3×10^7 electrons/cm^3. The measured average ion density under these conditions is about 6×10^6 ions/cm^3, so that the agreement is satisfactory.

D. Radio-Frequency Activity

Since the injection process in the present experiment results in a highly anisotropic and monoenergetic distribution of trapped ions, we expect to observe velocity-space instabilities. The approximate criterion for Harris-type[8] instability, $\omega_{pe} > \omega_{ci}$, is easily satisfied at our normal densities, and we do observe coherent oscillations at frequencies near ω_{ci} over the range of magnetic fields used. The intensity and continuity of the signals depend on the plasma density in an irregular way, but generally the intensity decreases, and the activity becomes more intermittent as the density decreases. With both the intensity and the duration of the rf signals varying, it is difficult to assign a number to the "strength" of the activity, and only qualitative statements can be made.

In the plasma density range $1\text{–}4 \times 10^7/\text{cm}^3$, the rf signal varies with magnetic field as shown in Fig. 14. There appear to be two different modes of activity, one at the lower fields characterized by an H_z polarization and the other at higher fields characterized by an H_θ polarization. In the intermediate range of fields, either type of activity may occur with H_θ at $2\omega_{ci}$. Occasionally, a mixture of the two components is seen. The H_z activity always occurs with a very narrow bandwidth ($\Delta f/f < 0.5\%$), while the H_θ activity has a large spread in frequency ($\Delta f/f \approx 1\text{–}5\%$). The magnetic field varies by about 5% within the plasma volume so that the H_z frequency band indicates a localized oscillation. Our magnetic field measurements are not precise enough

to correlate the observed frequency with a local value of ω_{ci}. The H_z activity is generally weaker than the H_θ. We have not been able to identify the observed modes with those listed by Hall *et al.*,[23] and it is clear that more detailed measurements would be necessary to complete our understanding of these activities.

The rf activity and the low-frequency flute oscillations are strongly coupled. One correlation between these signals has already been pointed out: At high magnetic fields the centered configuration is always associated with H_θ activity. The off-center distribution is usually without rf activity. We have adopted the explanation that the onset of H_θ rf oscillations is responsible for the flute configuration change through the ejection of electrons with subsequent increase in the plasma potential. While plausible, the cause-effect relation has not been proved.

A second correlation was mentioned in our earlier paper[18] and can now be restated in more detail. The dispersion relation for the flute oscillation has two solutions or branches, one in which the oscillation frequency is approximately independent of density and close to the ∇B precession frequency and the other in which the frequency is approximately proportional to density (see Fig. 13). The plasma usually chooses the first branch in the presence of H_θ activity or in the absence of observable rf activity. The second branch is usually chosen in the presence of H_z activity. The reasons for this correlation are obscure.

Finally, the rf signal, when continuous, is often modulated at the flute frequency, possibly because of the varying proximity of the rotating plasma to the antenna. Other random variations in rf amplitude are of course also seen.

Harmonics of ω_{ci}, other than the region of H_θ activity at $2\omega_{ci}$ shown in Fig. 14, have not been detected although searched for. We observed weak H_z activity at $\frac{1}{2}\omega_{ci}$ during one run but have not been able to reproduce this result. All rf signals seem to cease at magnetic fields above about 30 kG. In this region we may be reaching a condition where the ratio ω_{ci}/ω_{pe} becomes too high, exceeding the critical value for instability to occur.

V. DISCUSSION

The theoretical development presented in the Appendix, which is based on the observed inequality of electron and ion densities, yields a satisfactory explanation of both the observed density limits

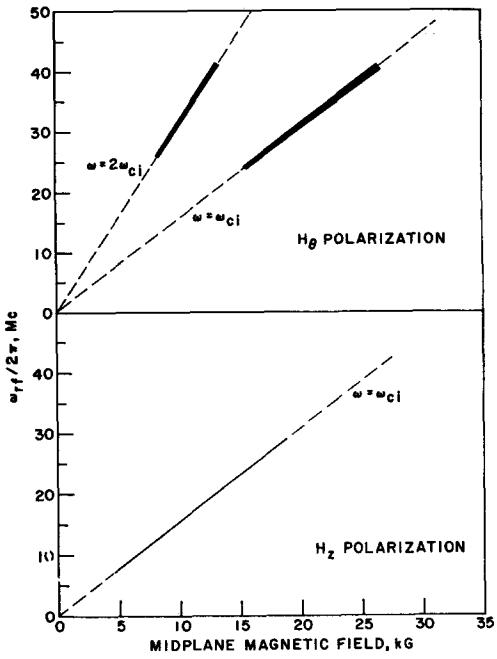

FIG. 14. Solid line segments show regions of rf activity observed with full beam and good vacuum ($I\tau_{cx} \gtrsim 1$ mA sec).

and the oscillation frequencies. From these comparisons, there is little doubt that the cause of the severe limitation of average plasma density is an $m = 1$ drift instability characteristic of the simple magnetic-mirror geometry. An additional proof of this interpretation is derived from the increase in density observed in the same apparatus when longitudinal line-cusp fields are added to the mirror field to create a "minimum-B" configuration with reversed field gradient. These results have been described elsewhere.[24]

The measured radial and azimuthal distributions of trapped ions cannot be derived from existing theory, and it would probably require a nonlinear treatment to describe the plasma in such detail. A derivation of the high plasma potential also remains outside of existing theory.

The gross properties of the plasma are not greatly affected by the axial distribution of ions, although this distribution appears to be related to the oscillation modes observed at the ion gyrofrequency. When the beam is injected with an axial displacement from the midplane which approximately doubles the axial extent of injected ions, no essential change is observed in either the drift instability or the gyrofrequency modes. More detailed measurements of the axial distribution remain to be made.

[23] L. S. Hall, W. Heckrotte, and T. Kammash, Phys. Rev. Letters **13**, 603 (1964).

[24] C. C. Damm, J. H. Foote, A. H. Futch, A. L. Gardner, and R. F. Post, Phys. Rev. Letters **13**, 464 (1964).

The energy of most of the trapped ions remains close to 20 keV as evidenced by analysis of the pulse height spectrum from the semiconductor detector of fast atoms. A shift in mean energy of about 1 keV or a spread in energy of several keV could be detected but is not observed. We cannot presently exclude the possibility that a small fraction of the ions which are not sufficient to produce an observable shift in the mean energy are undergoing an energy shift.

The resonance modes of oscillation observed at the ion gyrofrequency seem to be affecting the plasma mainly through coupling with the dominant low-frequency drift instability. The resulting complexity has so far prevented a clear analysis of these high-frequency modes. It is probable that a satisfactory study of the resonance modes can only occur after the flute oscillations are eliminated (for instance, in a "minimum-B" type field).

ACKNOWLEDGMENTS

We wish to acknowledge the continued support and encouragement of C. M. Van Atta. Engineering design was directed by W. Neef and A. Waugh. We wish to thank J. R. Hiskes for many helpful discussions on Lorentz ionization and W. Heckrotte, K. Neil, and L. Hall for discussions on various aspects of the theory. We are indebted to M. K. Bainter, T. P. Stack, and the rest of the operating staff for the assembly and operation of the apparatus. We thank the many technical specialists who worked with us to meet the exacting technological requirements of the experiment.

This work was done under the auspices of the U. S. Atomic Energy Commission.

APPENDIX. THE FLUTE INSTABILITY FOR A LOW-DENSITY PLASMA WITH UNEQUAL ION AND ELECTRON DENSITIES

Simple magnetohydrodynamic theory predicts interchange instabilities for a plasma confined by a magnetic mirror field.[4] Rosenbluth, Krall, and Rostoker[25] have modified this theory to include stabilizing effects resulting from the finite size of the ion orbit. This "finite orbit" theory has been extended to the low density region ($n \leq B^2/4\pi Mc^2$) by Mikhailovskii[5] and independently by Post.[6] The calculations of both Mikhailovskii and Post were in plane geometry. The effects of the magnetic mirror field were introduced by replacing the gravitational term with an equivalent acceleration due to the curvature of the magnetic field lines. This stability problem for a low density plasma has recently been solved in cylindrical geometry for which the acceleration resulting from the curvature of the field lines occurs naturally.[7] Finite orbit effects arising from drifts produced by the electric field were found to be small for densities of 10^8 particles/cm^3 and were neglected in evaluating the equations.

Equal ion and electron densities have been assumed for the unperturbed plasma in the foregoing papers. In the present theory, the treatment by Kuo and her co-workers has been modified by removing the assumption of quasi-neutrality of the unperturbed plasma. The resulting theory predicts an increase in the ion density at which the instability occurs as γ, the ratio of the electron density to the ion density, decreases. In the text of this paper, the present theory is compared with experimental results. This theory appears to give a reasonable explanation of the observed variation of the unstable density limit with changes in the plasma potential.

The electrostatic potential, Ψ, is determined from Poisson's equation:

$$-\nabla^2\Psi = 4\pi ec(n_+ - n_-), \tag{A1}$$

where n_+ and n_- are the perturbed ion and electron densities. These densities are calculated from the linearized continuity equations:

$$\frac{\partial n_+}{\partial t} + \mathbf{v}_+\cdot\nabla n_+ + \mathbf{v}_+'\cdot\nabla N_+ + N_+\nabla\cdot\mathbf{v}_+' = 0, \tag{A2}$$

$$\frac{\partial n_-}{\partial t} + \mathbf{v}_-\cdot\nabla n_- + \mathbf{v}_-'\cdot\nabla N_- + N_-\nabla\cdot\mathbf{v}_-' = 0. \tag{A3}$$

In Eqs. (A1) and (A2), $\mathbf{v}_\pm$ are the drift velocities of the particles due to both the magnetic field gradient and the $\mathbf{E}\times\mathbf{B}$ drift of the zero order electric field, $\mathbf{v}_\pm'$ are the perturbed velocities given by

$$\mathbf{v}_\pm' = \frac{\mathbf{E}_1\times\mathbf{B}}{B^2} + \frac{(\partial/\partial t + \mathbf{v}_\pm\cdot\nabla)\mathbf{E}Mc}{eB^2}, \tag{A4}$$

and $N_\pm$ are the unperturbed ion and electron densities.

The following forms for the electrostatic potential and the perturbed ion and electron densities are assumed:

$$\Psi = \psi(r)e^{i(\omega t+m\phi)}, \tag{A5}$$

$$n_+ = n_+(r)e^{i(\omega t+m\phi)}, \tag{A6}$$

$$n_- = n_-(r)e^{i(\omega t+m\phi)}. \tag{A7}$$

If one approximates the magnetic mirror field by

$$\mathbf{B} = \frac{B_0}{1+B_1r^2}\,\mathbf{z}_0, \tag{A8}$$

[25] M. N. Rosenbluth, N. A. Krall, and N. Rostoker, Nucl. Fusion Suppl. Pt. 1, 143 (1962).

then the gradient-B rotational frequency of the ions is given by

$$\Omega_M = \frac{c}{e}\frac{T}{B^2 r}\frac{dB}{dr} = -\frac{c}{e}\frac{2B_1 T}{B_0}, \quad \text{(A9)}$$

where T is the ion energy. The electric rotation frequency due to the zero order electric field is equal to

$$\Omega_E = -\frac{cE}{rB} = \frac{-4\pi ec(1-\gamma)}{Br^2}\int_0^r N_+ r'\,dr'. \quad \text{(A10)}$$

From Eqs. (A9) and (A10), one obtains

$$\mathbf{v}_+ = -\left[\frac{c}{e}\frac{2B_1 Tr}{B_0} + \frac{4\pi ec(1-\gamma)}{Br}\int_0^r N_+ r'\,dr'\right]\boldsymbol{\theta}_0. \quad \text{(A11)}$$

Since the low-energy electrons have negligible gradient-B drift, one obtains

$$\mathbf{v}_- = -\left[\frac{4\pi ec(1-\gamma)}{Br}\int_0^r N_+ r'\,dr'\right]\boldsymbol{\theta}_0 \quad \text{(A12)}$$

for the electron velocity.

With the foregoing assumptions, the perturbed ion and electron densities may be easily obtained from Eqs. (A2) and (A3) after substitution of Eqs. (A4), (A11), and (A12) for the particle velocities. If the perturbed densities are then substituted into Poisson's equation and terms of order ω/ω_{ci}, Ω_M/ω_{ci}, and Ω_E/ω_{ci} neglected, one obtains the equation

$$\frac{d^2\psi}{dr^2} + \frac{1}{r}\frac{d\psi}{dr} + \left\{-\frac{m^2}{r^2} + \frac{4\pi ec}{B}\left[\left(\frac{dN_+/dr}{\omega + m\Omega_T} - \frac{dN_-/dr}{\omega + m\Omega_E}\right)\frac{m}{r} - \frac{4m\Omega}{a^2\omega_c}\left(\frac{N_+}{\omega + m\Omega_T} - \frac{N_-}{\omega + m\Omega_E}\right)\right]\right\}\psi = 0 \quad \text{(A13)}$$

for low densities and magnetic fields above 5 kG for which $(4\pi Mc^2/B^2)N_+ \ll 1$.[26] In Eq. (A13) the total rotation frequency, Ω_T, is equal to the sum of the magnetic and electric rotation frequencies. If it is assumed both that N_+ and N_- have the same shape, i.e.,

$$N_- = \gamma N_+,$$
$$dN_-/dr = \gamma\, dN_+/dr,$$

where γ is a constant, then Eq. (A13) becomes

$$\frac{d^2\psi}{dr^2} + \frac{1}{r}\frac{d\psi}{dr} + \left(\alpha^2 - \frac{m^2}{r^2}\right)\psi = 0, \quad \text{(A14)}$$

where

$$\alpha^2 = \frac{4\pi ecm}{Br}\left[\frac{\omega + m\Omega_E - \gamma(\omega + m\Omega_T)}{(\omega + m\Omega_E)(\omega + m\Omega_T)}\right]\cdot\frac{dN_+}{dr}\left(1 - \frac{2\nabla \ln B}{\nabla \ln N_+}\right). \quad \text{(A15)}$$

We may now choose the plasma density distribution such that

$$\frac{1}{Br}\frac{dN_+}{dr}\left(1 - \frac{2\nabla \ln B}{\nabla \ln N_+}\right) \quad \text{(A16)}$$

is a constant. The distribution which satisfies this condition is

$$N_+ = \frac{N_0}{(1 + B_1 r^2)^2}\left[1 - \frac{r^2}{r_0^2}\frac{(1 + \frac{1}{2}B_1 r^2)}{(1 + \frac{1}{2}B_1 r_0^2)}\right], \quad \text{(A17)}$$

where r_0 is the plasma radius. This distribution differs only slightly from a parabolic distribution and reduces to the parabolic distribution for a constant magnetic field, i.e., when $B_1 = 0$.

For the particular case when $\gamma = 1$, then $\Omega_E = 0$ and α^2 is a constant independent of r. For this case the equation reduces to the results obtained by Kuo *et al.*[7] If in addition one neglects the $(\nabla \ln B)/(\nabla \ln N)$ term, then Eq. (A14) reduces to Kadomtsev's equation[27] for a parabolic density distribution. Both of these limiting cases result in Bessel's equation which is easily solved for the characteristic eigenfrequencies.

In general α^2 is a function of r and numerical methods are necessary to obtain solutions; however, if $\Omega_E(r)$ is replaced by its average value over the plasma volume, α^2 is again constant and the potential inside the plasma is given approximately by[28]

$$\psi = AJ_m(\alpha r)\cos(\omega t + m\phi). \quad \text{(A18)}$$

The parameter α is determined from the requirement that the potential be zero at the chamber walls. The dispersion relation becomes

$$\omega = -\tfrac{1}{2}[m(\Omega_M + 2\Omega_E) + (1-\gamma)D/\alpha^2] \pm \tfrac{1}{2}\{[m\Omega_M + (1-\gamma)D/\alpha^2]^2 + 4m\Omega_M\gamma D/\alpha^2\}^{\frac{1}{2}}, \quad \text{(A19)}$$

where

$$D = \frac{8\pi ecmN_0}{B_0 r_0^2(1 + \frac{1}{2}B_1 r_0^2)}. \quad \text{(A20)}$$

For $m = 1$ the plasma becomes unstable when

$$D > \frac{\alpha^2}{4\gamma\,|\Omega_M|}\left[-|\Omega_M| + \frac{D}{\alpha^2}(1-\gamma)\right]^2. \quad \text{(A21)}$$

[26] Substituting the perturbed density of the guiding center from the continuity equations into Poisson's equation, which is only applicable to particle density, is equivalent to neglecting the finite size of the particle orbits. It is easily shown that the error made by this substitution is small for low densities and magnetic fields above 5 kG.

[27] B. B. Kadomtsev, Zh. Eksperim. i Teor. Fiz. **40**, 328 (1961) [English transl.: Soviet Phys.—JETP **13**, 223 (1961)].

[28] The plasma stability conditions determined by this approximation are in good agreement with exact solutions of the basic equations obtained by numerical methods. The numerical calculation will be reported in a separate publication.

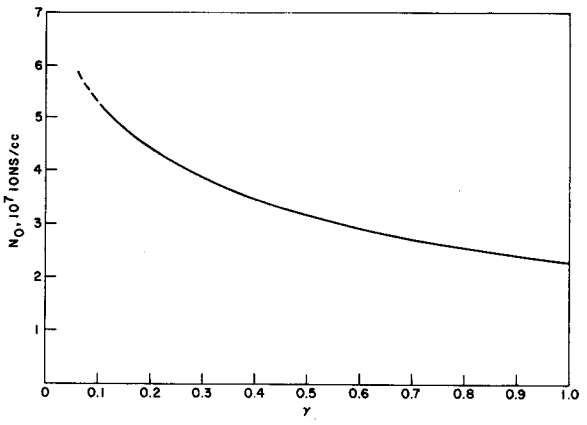

FIG. 15. Density for which the plasma becomes unstable versus the ratio of electron to ion density, γ.

Using the following typical parameters for the Alice plasma,

$$r_0 = 15 \text{ cm}, \qquad B_1 = 5.3 \times 10^{-4},$$
$$\alpha = 0.256, \qquad D = 1.517\, N_0/B_0,$$
$$|\Omega_M| = (c/e)T(2B_1/B_0) = 212 \times 10^7/B_0,$$

Eq. (A21) becomes

$$N_0 > \frac{2.291 \times 10^7}{\gamma} [-1 + 10.95 \times 10^{-9} N_0(1 - \gamma)]^2. \tag{A22}$$

The density for which the plasma becomes unstable as predicted by Eq. (A22) is shown plotted in Fig. 15.

THE PHYSICS OF FLUIDS VOLUME 8, NUMBER 8 AUGUST 1965

Universal Instability in Complex Field Geometries

NICHOLAS A. KRALL AND MARSHALL N. ROSENBLUTH*
General Atomic Division of General Dynamics Corporation,
John Jay Hopkins Laboratory for Pure and Applied Science,
San Diego, California
(Received 30 November 1964; final manuscript received 22 March 1965)

An inhomogeneous collisionless plasma in a magnetic field **B** is unstable to an electrostatic oscillation propagating nearly perpendicular to **B** but with a large phase velocity parallel to **B**. We study the stability of this mode in a more complicated plasma equilibrium, including magnetic shear, finite plasma length, currents parallel to **B**, temperature gradients, and gravity-simulated magnetic cusp or mirror curvature. We find that many of these equilibria are stable to this mode, which has been misnamed a "universal instability."

I. INTRODUCTION

A COLLISIONLESS plasma in equilibrium with a nonuniform magnetic field $\mathbf{B} = B(x)\hat{n}_z$ exhibits a number of modes[1-8] of oscillation characterized by a group velocity nearly perpendicular to the magnetic field. This group velocity is similar in size and direction to that of drifts

$$V_D = \frac{1}{2}\frac{\nabla B}{B}\left(\frac{mc}{eB}\right)V_\perp^2$$

and currents

$$V_c = \frac{1}{2}\frac{\nabla n}{n}\left(\frac{mc}{eB}\right)V_\perp^2$$

set up in the plasma by the nonuniformity of **B**.[9] Among these modes are stable waves, unstable waves, electrostatic, mixed, and transverse waves, and all are strongly affected by increasing the complexity of the plasma equilibrium, i.e., including shear fields, including gravity to simulate cusp or mirror geometry, including temperature gradients, currents parallel to **B**, finite Larmor radius effects, etc.

* Also at the University of California, San Diego, La Jolla, California.

[1] N. A. Krall and M. N. Rosenbluth, Phys. Fluids **6**, 254 (1963).

[2] L. I. Rudakov and R. Sagdeev, Zh. Eksperim. i Teor. Fiz. **37**, 1337 (1959) [English transl.: Soviet Phys.—JETP **10**, 952 (1960)].

[3] M. N. Rosenbluth, N. A. Krall, and N. Rostoker, Nucl. Fusion Suppl. Pt. 1, 143 (1962).

[4] N. A. Krall and M. N. Rosenbluth, Phys. Fluids **5**, 1435 (1962).

[5] M. N. Rosenbluth, Report of the Culham Laboratory Study Group on Plasma Instabilities, CLM-M21 (1963).

[6] A. B. Mikhaĭlovskiĭ and L. I. Rudakov, Zh. Eksperim. i Teor. Fiz. **44**, 912 (1963) [English transl.: Soviet Physics—JETP **17**, 621 (1963)].

[7] B. B. Kadomtsev and A. V. Timofeev, Dokl. Akad. Nauk. SSSR **146**, 581 (1962) [English transl.: Soviet Phys.—Doklady **7**, 826 (1963)].

[8] B. B. Kadomtsev, J. Nucl. Energy **C5**, 31 (1963).

[9] S. Chandrasekhar, *Plasma Physics* (University of Chicago Press, Chicago, Illinois, 1960).